TM-918
8035.000
October 1979

The Electron Beam for the Fermilab Electron Cooling Experiment

I. Initial Operation and Studies

W. Kells, P. McIntyre, L. Oleksiuk
Fermilab

N. Dikansky, I. Meshkov, V. Parkhomchuk
Institute for Nuclear Physics Novosibrisk, USSR

W. Herrmannsfeldt
SLAC

1. Electron Cooling Region

The electron cooling of the stored proton beam occurs in the straight sections shown in Figure 1. The design must provide a cold, intense electron beam and bring it into near perfect alignment with the proton beam. The electrons are confined in the drift region by a 1 kG solenoidal magnetic field to avoid divergence produced by space charge forces.

Electron Gun

The electron beam must have a rest frame temperature $T_e < 1$ eV. To produce such a low temperature, the electron gun has been designed with a classic Pierce geometry, and is itself immersed in the magnetic field. This means that the magnetic field lines thread through the cathode, and follow the electron trajectories all the way to the collector. Otherwise, the electrons would gyrate around the actual magnetic field direction, and increase greatly the transverse temperature. We have chosen to use the electron gun design developed for the SPEAR klystron. It produces a 28A, 27 cm^2 beam at 110 kV. The dispenser cathode can be reactivated repeatedly after exposure to air. The defocusing lens action of the anode causes the electrons to spiral, resulting in the undulation. This undulation is cancelled by a "resonant" focusing system of three electrodes. Electrode potentials are adjusted to match the spiral motion so that the electrons emerge parallel.

Drift Region

After leaving the gun, the beam is bent 90^0 to superimpose it on the proton beam. The bending is accomplished with a crossed toroidal and dipole magnetic field. The resulting trajectory bends through a circular arc without exciting gyrations. The toroid has a gradient of 6.7 kG/m, and a dipole field of 80 G.

The cooling will take place in a 5 m long drift region, where the electron beam is confined by a uniform-field solenoid. We have chosen a solenoidal field B_0 = 1 kG as being adequate both for beam confinement and for studying "fast" cooling. The solenoid is an assembly of 0.5 m long coils of anodized aluminum strip conductor. The field produced by a long sequence of the coils with minimum spacing has a uniformity $(\delta B/B)_{rms} \leq 5 \times 10^{-4}$, sufficient for optimal electron cooling.

The ground potential surface throughout the bending and cooling region is a drift tube of 6" diameter. This drift tube is split longitudinally into segments, and each segment is connected to an independent voltage source (see Figure 1). By depressing the "ground" in the cooling region several kV below the ground in the short drift sections in each 60^0 bend, it is possible to trap the ions formed by beam gas scattering in the cooling regions, and neutralize the space charge in the electron beam. The ion density needed has an equivalent pressure of

$$P_i = \frac{1.6 \times 10^{-8}\ \text{Torr}}{Z}$$

Depressed Collector

After a second 90^0 bend, the beam is decelerated and absorbed in a collector assembly. It is essential to recover as much as possible of the beam power

(2.6 MW) for realistic collection and optimum beam regulation. For this purpose the collector is operated at a potential only slightly ($\delta E \sim$ few kV) lower than that of the electron gun cathode. The collection is then efficient only if no electrons have lost more than δE of energy since their birth at the gun cathode. Any energy coupled to gyration in the deceleration process is difficult to recover into longitudinal motion. One difficulty in maximizing the collection efficiency at the collector is secondary emission and backscattering from the collector surface.

II. Electron Beam Studies

We present here a chronological history of electron beam studies to date. The studies divide logically into two periods. In the first period, we studied beam performance in the energy range 0 - 5 kV, with strong deceleration in the collector: the collector anode was at ground potential, so that the beam decelerates fully in the collector. In the second period, we studied beam performance in the energy range 0 - 20 kV, with weak deceleration in the collector: the collector anode was held near cathode potential, so that most deceleration occurs upstream of the collector.

Period I: V_{gc} = 0 - 5 kV V_{ga} = 0, V_{ca} = 0, V_{cc} = 1.3 - 4 kV, $P \sim 2 \times 10^{-6}$ Torr, $I_{cc} \sim$ 0 - .25A, $\varepsilon \gtrsim$ 3-5%.

Figure 2 shows the fractional beam loss I_ℓ/I_e observed as a function of collector depression V_{cc} and for comparison, the losses predicted from ionization currents created in the residual gas.

Initially beam current was limited by reducing cathode temperature. We studied the steering alignment of the beam through the drift structures, using mainly the dipole steering coils. We observed surface charging on drift tubes;

when the beam would scrape a drift tube, it would charge up to a negative voltage $\lesssim V_{gc}$, and further perturb the beam until the steering element was tuned far in the reverse direction, generating an apparent hysteresis in the steering curves. This was a result of the single quadrant design of the power supplies used for electrodes, anodes, and drift tubes. Each supply could sink current to bring a load from ground to the desired voltage; but it could not source current to prevent a load from going more negative then the desired voltage, due to beam interception current. All anodes, electrodes and drift tubes were grounded, and the beam was operated as a diode switch tube.

We observed light emitted along the long drift tube originating from gas scintillation in the beam. The light was correlated with wall losses when we steered the beam in the drift structures.

Several aspects of beam steering studies were disquieting. First, several steering curves (particularly H3, V3) did not appear to have a flat region with minimum loss. This would suggest an aperture limitation. Second, an optimally steered beam would still have a loss fraction $\varepsilon \sim$ 3-5%, with at least 80% of the remaining losses occuring roughly equally at the two anodes (I_{ga}, I_{ca}). The anodes represent the smallest apertures to the beam, so this led us to suspect that the peripheral rays were scraping the anodes.

The origin of losses became clear late in this period when we began to operate the gun with space charge limited emission. We observed (Figure 3) that

$$I_e = I_o - n I_L$$

Thus the newly emitted (and collected) current I_e is reduced from its no-loss value by the space charge from n passages of the lost beam I_L. That can only

be the case if the lost beam bounces back and forth n times (on the average) between gun and collector before intercepting an anode. Thus the losses occur naturally at the anodes; the lack of a flat bottom to the steering curves is due to the slow growth of the reflected component, and not to an aperture limitation.

Period II: V_{gc} = 0 - 20 kV, V_{ga} = 0, V_{ca} = 0 - 20 kV, V_{cc} = 1.3 - 4 kV, P $\sim 10^{-8}$ Torr, I_{cc} = 0 - 2A, $\varepsilon \lesssim 2 \times 10^{-4}$.

After period I, it remained to understand why a fraction $\varepsilon \sim$ 3-5% of the beam was reflected from the collector. To study the collection process, it was necessary to vary V_{ca}. A cathode follower circuit was designed to provide second quadrant regulation for the V_{ca} supply. This technique succeeded, so that V_{ca} could be set and stabilized at any desired voltage. We then observed a dramatic improvement in collection losses when the collector anode was operated near cathode potential, $V_{ca} \lesssim V_{gc}$. The losses I_L drop rapidly as V_{ca} approaches V_{gc} (Figure 4), until finally the beam blows up. The losses are $\varepsilon \sim 2 \times 10^{-4}$ for V_{gc} = 20 kV, I_e = 2A.

This behavior was startling in view of our Poisson calculations of the beam in the collector region. The electron space charge for a 2A beam should produce $\sim$ 5 kV depression in the aperature of the collector, and prevent collection of central rays for $V_{ca} \gtrsim V_{gc}$ - 5 kV. The observed improvement for large V_{ca} signals the presence of a stable cloud of slow gas ions, which are formed and trapped in the potential well near the collector anode, and which partially neutralizes the electron beam as it decelerates.

Ion trapping in the collector region has not been reported in electron beams at Novosibirsk and CERN. The dramatic effect of losses must result from a strong, uniform potential barrier to suppress electrons backscattered from

the collector surface. This conclusion is substantiated in Poisson calculations which include ion neutralization.

The optimum collection efficiency is not strongly dependent on collector depression V_{cc} (see Figure 5). We interpret this to mean that, while the topology of the equipotentials is altered by an ion cloud, the total depression in front of the collector wall scales with V_{cc}, and suppresses backscattered electrons independent of V_{cc}.

III. Ion Compensation

In order to understand the observed effects of ion compensation in the collector region, it is necessary to calculate the space charge potential distribution that is developed there. This can be done using the self-consistent solution of electric potentials arising from the Poisson equation:

$$\nabla^2 \varphi = \frac{J_e}{\varepsilon_o \sqrt{\frac{2e}{m}\varphi}} \qquad (1)$$

where J_e is current density,
m is electron mass
e is electron charge
ϕ is potential w.r.t. cathode (kinetic energy)

From the solution of equation (1), for a 2 amp, 5 cm. diam. electron beam traveling in a 8 cm. diam. anode, a minimum kinetic energy of 150 volts is predicted for the central electron ray, with the anode voltage off set (ΔV_{ca} - V_{gc}) at 3 kV. This condition defines the minimum anode potential, below which the primary beam is reflected because of beam space charge. The cup voltage must then be above this to provide suppression of secondary emission and backscattering.

Successful collection of a 2 ampere x 20 KV electron beam was achieved with a collector voltage of 1.3 kV, and anode voltage of 0.8 kV. Computer modeling calculations of this beam collection mode predict a negative kinetic energy of 1.14 kV, (Figure 6) implying full beam reflection resulting from the space charge developed in the anode.

The apparent attenuation of the space charge depression can be understood in terms of an ion trapping process in the potential well produced by the primary beam. Ions formed within regions with potentials lower than the surrounding electrode potential will be trapped in closed regions, thus neutralizing the electron space charge.

Ions are trapped in the collector region only when the electron current is sufficient to produce closed potential wells due to space charge. The initial defocusing transverse electric field arising from the electrode structure is given by:

$$E_\perp^\circ = \frac{1}{2}\frac{\partial^2 \varphi}{\partial z^2} r \quad r > 0 \tag{2}$$

while the transverse electric field arising from the ion compensated space charge is:

$$E_\perp = -\frac{J_e}{2\varepsilon_0}\cdot\frac{r}{\sqrt{\frac{2e}{m}\varphi}} + \frac{n_i e r}{2\varepsilon_0} \tag{3}$$

where n_i is the ion density

For ion trapping we require:

$$E_\perp^\circ + E_\perp \leq 0 \tag{6}$$

Thus the threshold condition for ion trapping is defined by a minimum electron beam current, assuming a fixed ion density. When the ion compensation makes the net transverse electric field = 0, the resulting axial potential distribution satisfies:

$$\varphi(z) = \varphi_0(z) - \frac{1}{2}\frac{\partial^2 \varphi}{\partial z^2} a^2 \log(R/a) \qquad (5)$$

where R is the wall radius,
$\phi_0(z)$ is the (Laplace) potential without the beam

Equation (5) implies that effective ion compensation requires slowly changing axial electric fields.

The net ion population under trapping conditions is a stable equilibrium of the ion production rate, balanced against the ion losses due to diffusion to the walls. The ion production rate is given by:

$$\frac{dn_i}{dt} = n_0 \frac{\pi e^4}{m E_i} n_e v_e \qquad (6)$$

where n_0 is the density of the residual gas

E_i is the ionization energy of the residual gas

(n_e, v_e) are electron density, velocity respectively

The diffusion of the ions is generated by electron heating. This heating rate is given by:

$$\left(\frac{dE}{dt}\right)_{ion} = \frac{\pi e^4 n_e}{M_i v_e} L \qquad (7)$$

where L is the coulomb logarithm, and

M_i is the ion mass

The resulting diffusion rate is given by:

$$\frac{dn_i}{dt} = -\frac{1}{e(\varphi_w - \varphi_b)} \frac{dE}{dt} n_i \qquad (8)$$

where the potential drop from beam edge to wall is

$$(\varphi_w - \varphi_b) = \frac{e(n_e - n_i)}{2\varepsilon_0} a^2 \left(1 + 2\log(R/r)\right) \quad (9)$$

From the above relations an effective compensation ratio can be defined by:

$$\frac{n_e - n_i}{n_i} = \frac{E_i}{M_i c^2} \left\{ \frac{L}{r_e a^2 n_0 \pi \left(1 + 2\log(R/r)\right)} \right\} \quad (10)$$

where r_e is the classical electron radius

For residual gas pressures of 10^{-10} Torr, the resulting ion compensation ratio is 6×10^{-3}. The growth rate for ion compensation at this pressure is approximately 50 seconds.

It is interesting to note that the space charge compensation rate is independent of beam energy. Such compensation can also be useful, for example, in improving the damping conditions available in the cooling straight section.

Computer modeling of a good ion trapping geometry was performed, using the necessary conditions described above. A suitable geometry was obtained, as shown in Figure 7. Ion compensation and collection were simulated under beam conditions of 110 kV, 25 amperes. The design of the electrode geometry was determined by the requirement of effective secondary suppression of emission, and backscattering, consistent with formation of a stable ion trapping potential well.

The ion neutralization effects were modeled by allowing net space charge density to approach zero within bounded regions whose potential was near the minimum wall potential. Figure 7 shows the modeled potential map produced in the collector when ion neutralization is assumed for a 900 volt equipotential region, with surrounding electrodes at 5 kV (collector) and 1 kV (anode).

The calculated net axial charge density is shown, defining the region where ion trapping occurs. The increasing charge density near the trapping region arises from the strong deceleration of the primary beam. The charge density abruptly vanishes at the edge of the trapping region.

The resulting potential distribution left near the cup surface after neutralization provides a suppression voltage of about 4 KV, producing very efficient beam collection.

IV. Electron Losses and Instabilities in Collector

Our principle method of detecting a plasma instability at the collector anode is an antenna system in the long electron cooling straight section. This pick up system was designed to pick up microwave noise generated by transverse (cyclotron) motion of the primary electron beam. The form and location of the antenna is sketched in Figure 8. An important point is that the antenna is far from the anodes. Thus it is sensitive only to coherent bunches of reflected electrons bouncing between anodes, and not to radiation directly from the anode regions. Since the pick up system was designed to operate between 2 and 4 GHz our measurements of low frequency spectra are with a very low and poorly understood sensitivity (as a function of frequency). We can only roughly calculate the integrated power in the RF spectra described below.

Initially we looked for microwave signals at the cyclotron frequency, expecting to observe the characteristic modes predicted as a function of beam energy and solenoid magnetic field. Immediately it was observed that an anomolously large signal appeared which was a strong function of beam loss fraction. Realizing that electron loss (especially loss detectable in the 5m drift region) would probably be associated with electrons reflecting between gun and collector

anodes, we looked for the low frequencies (∿ few MHz) characteristic of the bounce period. With simplified pick-up electronics (no microwave preamplifier or mixer) we indeed indentified the loss-associated spectra as being low frequency (3 - 700 MHz).

On a frequency scale of 0 - 1000 MHz we observed the broad envelope spectrum of Figure 9. This figure superimposes spectra corresponding to two values of loss current. The spectrum for 2mA loss illustrates a signal compatabile with circuit noise background alone. The loss current was varied by changing collector anode voltage. On a finer scale, the spectrum for 5mA loss current is seen to be a comb of harmonics, the first few of which are illustrated in Figure 10.

The harmonic structure is easily explained. Within the limit of measurement accuracy the fundamental period is just twice the gun-collector transit time. To check this we measured spectra at three beam voltages. A plot of electron velocity versus the measured harmonic spacing is presented in Figure 11.

The FWHM of the harmonic peaks can be used as a measure of the life time of lost electrons within the system (i.e., number n of bounces back & forth between gun and collector). Using the measured FWHM (Δf) we arrive at:

$$n \equiv \#_{bounces} = f/\Delta f \simeq 8 \cdot 8 \qquad (11)$$

This result is consistent with the calculation on the observed I_{beam} vs. I_{loss} described earlier (see Figure 3). In a space charge limited gun emission regime the charge density in the gun space charge cloud is a constant (at fixed voltage). This space charge comes from two source: first the fresh beam emitted from the cathode; second the charge of the lost, bouncing, electrons

at their turning point in the gun. The net condition is thus $I_e = I_o - n\, I_\ell$. Figure 5 shows this beam current "sag" as I_{loss} increases. Quantitatively the data of I_{beam} vs. I_{loss} yields n = 7.7.

The onset of UHF signals with I_{loss} is abrupt. This is fully illustrated in Figure 12. We identify the threshold of nonlinear RF power generation with the onset of a collective instability within the high intensity electron plasma near the collector. For a beam current of $\sim$ 2 amp and a collector anode voltage of 0.9 KV we calculate a plasma frequency $\gtrsim$ 200 MHz. We see from Figure 9 that the spectrum of harmonics extends up to $\sim$ 500 MHz. We achieve lowest losses by minimizing the collector anode voltage. Notice that this is also the condition for maximizing the anode region in the electron density and minimizing the UHF signals. The instability threshold therefore is not associated with a beam current limitation.

What about the microwave signals ($\gtrsim$ 1000 MHz) for which the pick up system was designed? When losses are minimized (UHF signal disappears) we find a residual signal corresponding roughly to the expected Doppler broadened cyclotron freqeuncy band (Figure 13). This residual remains constant for variations in I_{loss} for $I_{loss} \lesssim$ 3mA.

Theoretical Discussion of Instabilities

We achieve very low loss fractions because the electron beam space charge depression has been neutralized by trapped ions in the collector anode region. Thus it is essential to understand the condition for maintaining such trapped ions. In particular we calculate the stability of such a region of thermal ions under the excitation of the electron beam which passes through it. By

conservation of energy the longitudinal momentum imparted to an ion by an electron scattering is:

$$\Delta p_{\parallel}(ion) = \frac{\left(\Delta P_{\perp}(e^-)\right)^2}{2m v_o} \tag{12}$$

In the general magnetized case an electron spirals through the electrostatic field region of trapped ions. An integral $\Delta P_{\perp}$ is imparted. We can write an exact expression for this net imparted transverse momentum:

$$\Delta P_{\perp} = \frac{2\pi \bar{n}_i \ell r e^2}{v_o} \left| \int_{-\ell/2}^{\ell/2} \frac{n_i(z)}{\bar{n}_i} e^{i\omega z/v_o} \frac{dz}{\ell} \right| \tag{13}$$

where

n_i = density of ions in trap

ℓ = length of trap

v_o = electron velocity

ω = gyro frequency

The exponential ($e^{i\omega z/v_o}$) properly takes into account the magnetized motion. In order to calculate the net force on an ion ($dP_{\parallel}/dt$) we substitute (13) into (12) and integrate over all electrons in the beam:

$$F_{\parallel}(ion) = \int_o^a \frac{\Delta P_{\perp}^2}{2m v_o} n_e \left(2\pi r v_o dr\right) \tag{14}$$

where a = beam radius

This characteristic friction force decreases with increasing v_o, and leads to the so called "electron wind" instability (Ya. Derbenev, A. Skrinsky). The increment of the instability is:

$$\tau^{-1} = -\frac{1}{M_i}\frac{\partial F_{\parallel}}{\partial v_i} = \frac{N_i 2\pi r_i r_e n_e c}{\beta^3}\left|\int_{-\ell/2}^{\ell/2}(\quad)dz\right|^2 \qquad (15)$$

where $N_i = \pi n_i a^2 \ell$ = total number of ions trapped in the anode region; r_i and r_e are the ion and electron classical radii respectively. Using parameters of our recent studies (I_{beam} = 2A, $V_{anode} - V_{cathode} \gtrsim$ 1 kV, n_e = $3.3 \times 10^8/cm^3$, a = 2.5 cm $N_i = 3.2 \times 10^{10}$, $\ell \gtrsim$ 5 cm) and for no solenoidal field $\tau^{-1} = 3.6 \times 10^5/s$. Using an approximate longitudinal trapping potential in the anode of $V = V_0\left(1+\left(z/A\right)^2\right)$ with V_0 = 1 KV, A = 10cm we find an oscillation frequency = 0.7 MHz. Clearly a condition for there to be a coherent oscillation of the ions is that the spread of natural frequencies possible in the trapping well be less than the driving rate τ^{-1}. We see that it is impossible to trap ions in a collector configuration using zero solenoidal field (e.g., the Novosibirsk and CERN collectors).

On the other hand the integral in Eqn. (15) is very small for non zero solenoidal fields. Intuitively this is because: first the Larmor periods longitudinally are very short for $\sim$ 1 KV electrons in $\gtrsim$ 500 gauss ($\chi \sim$ 0.21 cm); and secondly no net transverse momentum is transfered to an electron when it transits an electrostatic field region in the adiabatic limit ($\chi << \ell$). If we use a model ion longitudinal distribution then we can perform the integral in (15), obtaining

$$\tau^{-1}(B) = \tau^{-1}(B=0)\, e^{-\omega^2\ell^2/v_0^2} \qquad (16)$$

For a case ℓ = 7cm τ^{-1}(B = 500G) = 1.2×10^{-10}.

As mentioned previously the observed instability must be associated with the electron plasma frequency for densities corresponding to those in the collector anode region. The precise mechanism for the onset of this oscillation remains unexplained.

In stable operation (lowest collector anode voltage) secondary electron emission from the collector is reflected back to the collector. With the onset of an electron space charge oscillation (against the trapped ion background) this reflection potential barrier oscillates in height, allowing the secondary emission net loss to vary at the plasma frequency.

As the collector anode voltage is raised potential gradients in the collector region change and secondary backstreaming loss increases. We cannot now distinguish which of these changes destabilizes the electron space charge. It is plausible that the potential gradients in the space charge region determine its Landau stability. On the other hand increased backstreaming must, at some level of loss, induce a "two stream" instability.

Concluding Remarks

From these studies it can be seen that ion neutralization of space charge must be taken into account in order to produce high efficiency beam collection. Under certain conditions, ion compensation can actually destroy the usual suppression of secondary emission due to electron beam space charge. However, by moving the ion trapping region outside the collector cup, ion neutralization can be exploited to produce very low power beam collection (with very small beam loss).

Bibliography

1. The Fermilab electron cooler is described in: "Fermilab Electron Cooling Experiment Design Report," J. Bridges, et. al., August 1978.

2. The Novosibirsk electron beam device and its performance are described in: V. I. Kudelainen, I. N. Meshkov and R. A. Salimov, Preprint INP-72-70, Novosibirsk (1970). See also an English translation summary in CERN report 77-08; April 13, 1977.

3. The "Electron Wind" instability is evaluated in Ya. Derbenev, A. Strinsky- Particle Accelerators 8 pp. 1-20, 1978.

4. The CERN electron cooler and its performance are reported in M. Bell, J. E. Chaney, F. Krienen and P. Moller Peterson, CERN $\bar{p}$-Lear-Note 29, 15·2.1979.

Figure Captions.

Figure 1. Electron beam system: (a) electric field elements
(b) magnetic field elements

Figure 2. Total beam current, and predicted loss from ionization, vs beam energy.

Figure 3. Electron beam current and loss current vs. collector anode voltage.

Figure 4. Electron beam current and loss current with ion compensation.

Figure 5. Loss fraction vs. anode voltage for V_{cc}=1.3 kV, 4 kV.

Figure 6. Negative kinetic energy region predicted for 20 kV, 2 A electron beam.

Figure 7. Ion compensation region and charge density predicted for 20 kV, 2 A beam.

Figure 8. Microwave pickup geometry in long straight section.

Figure 9. 0-1000 MHz spectrum of r.f. signal for 2 mA, 5 mA loss current. Total beam current is 2 A.

Figure 10. Fine structure spectrum of Figure 9.

Figure 11. Electron velocity vs. harmonic spacing in r.f. spectrum.

Figure 12. Dependence of r.f. power on beam losses.

Figure 13. r.f. spectrum of the Doppler broadened cyclotron radiatio

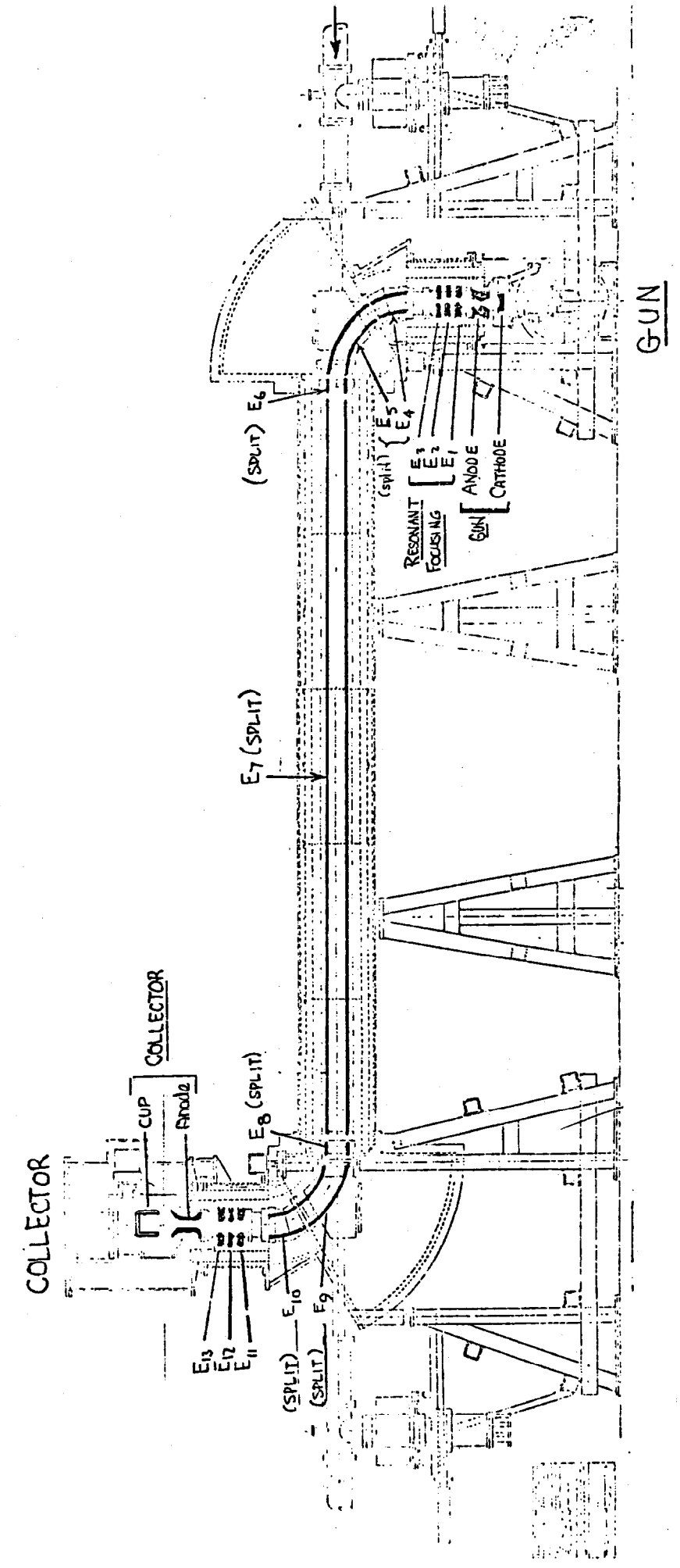
ELECTRON BEAM - E-ELECTRODES
GUN
COLLECTOR
COLLECTOR
CUP
Anode
E8 (SPLIT)
E7 (SPLIT)
(SPLIT) E6
(split) E5 E4
E3 E2 E1
RESONANT FOCUSING GUN
ANODE
CATHODE
E13 E12 E11
(SPLIT)
E10
(SPLIT)
E9

Figure 1a.

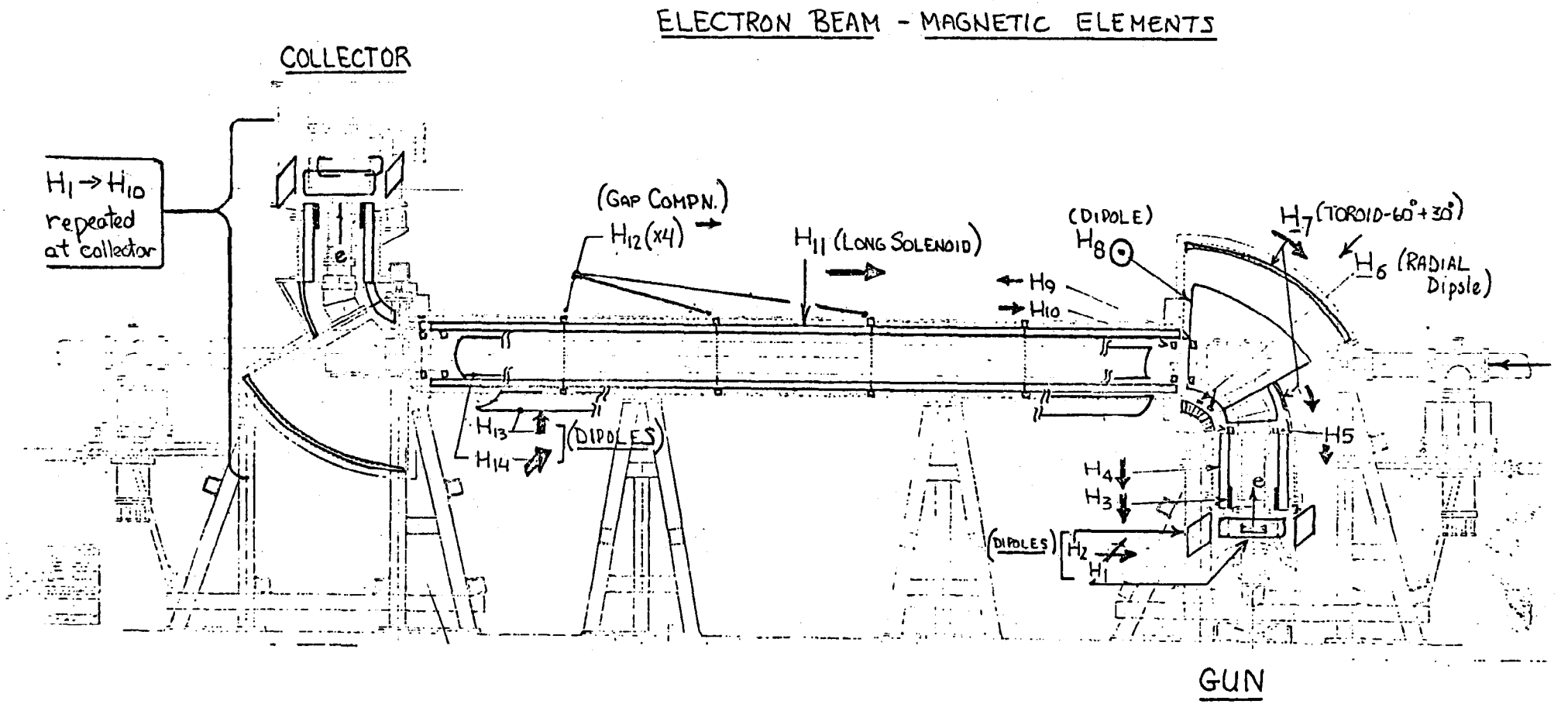
ELECTRON BEAM - MAGNETIC ELEMENTS
COLLECTOR
H1 → H10 repeated at collector
(GAP COMPN.)
H12 (x4)
H11 (LONG SOLENOID)
(DIPOLE)
H8
H7 (TOROID-60°+30°)
H6 (RADIAL Dipsle)
H9
H10
H13
H14
(DIPOLES)
H5
H4
H3
(DIPOLES)
H2
H1
GUN

Figure 1b.

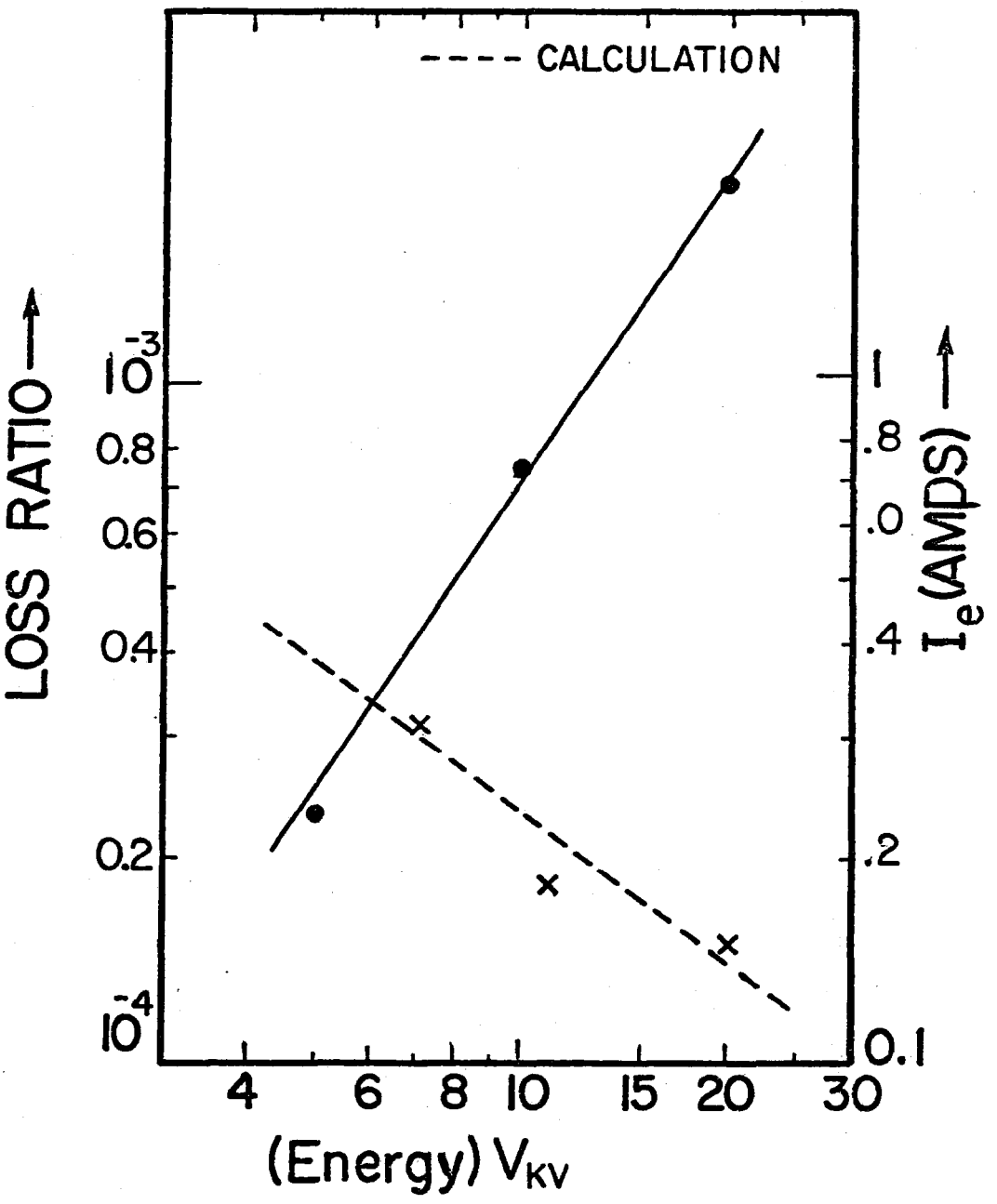
CALCULATION
LOSS RATIO
10^{-3}
0.8
0.6
0.4
0.2
10^{-4}
I_e (AMPS)
1
.8
.0
.4
.2
0.1
4
6
8
10
15
20
30
(Energy) V_{KV}

Figure 2

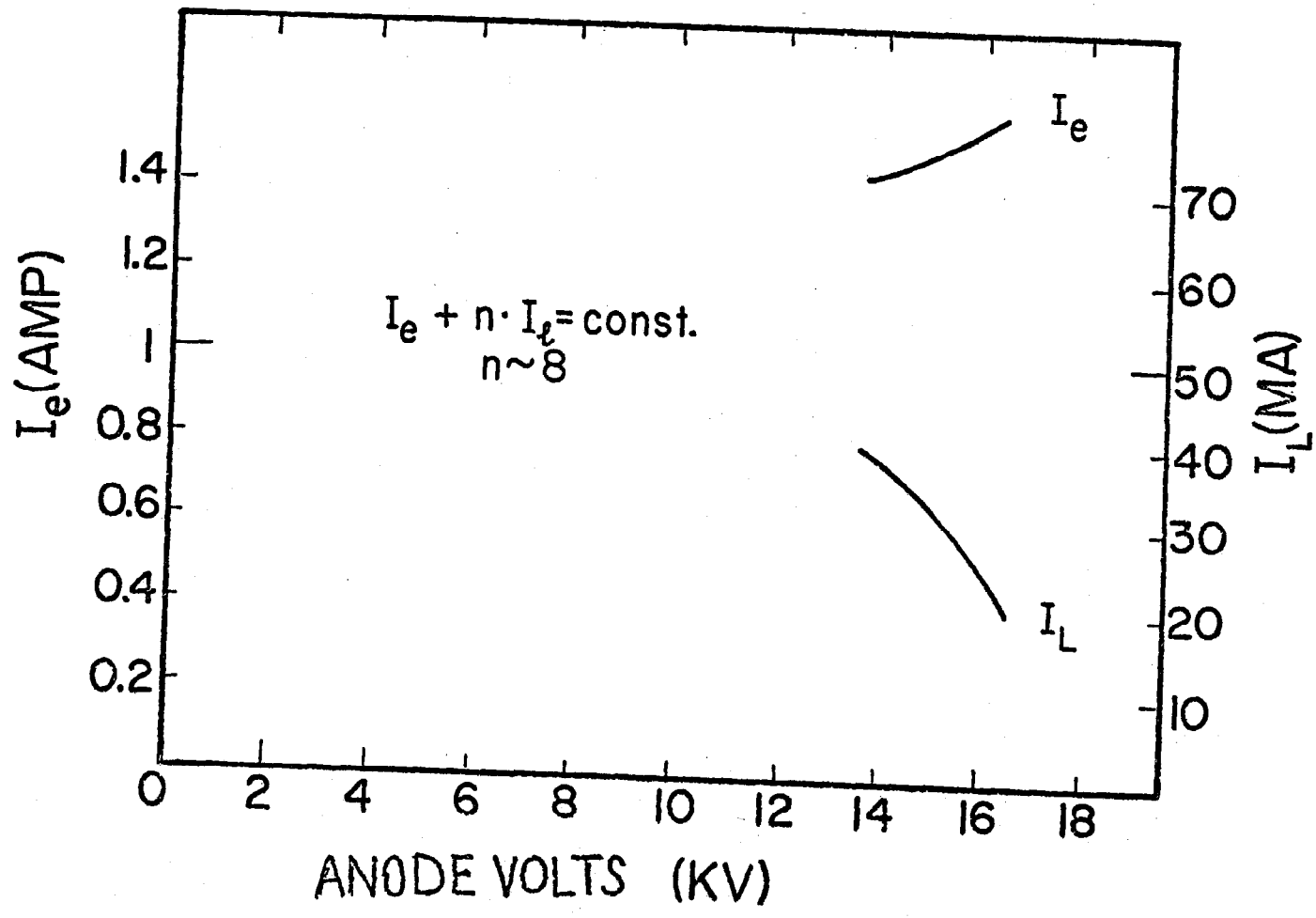
I_e
I_L
$I_e + n \cdot I_L = \text{const.}$
$n \sim 8$
I_e(AMP)
I_L(MA)
1.4
1.2
1
0.8
0.6
0.4
0.2
70
60
50
40
30
20
10
0
2
4
6
8
10
12
14
16
18
ANODE VOLTS (KV)

Figure 3

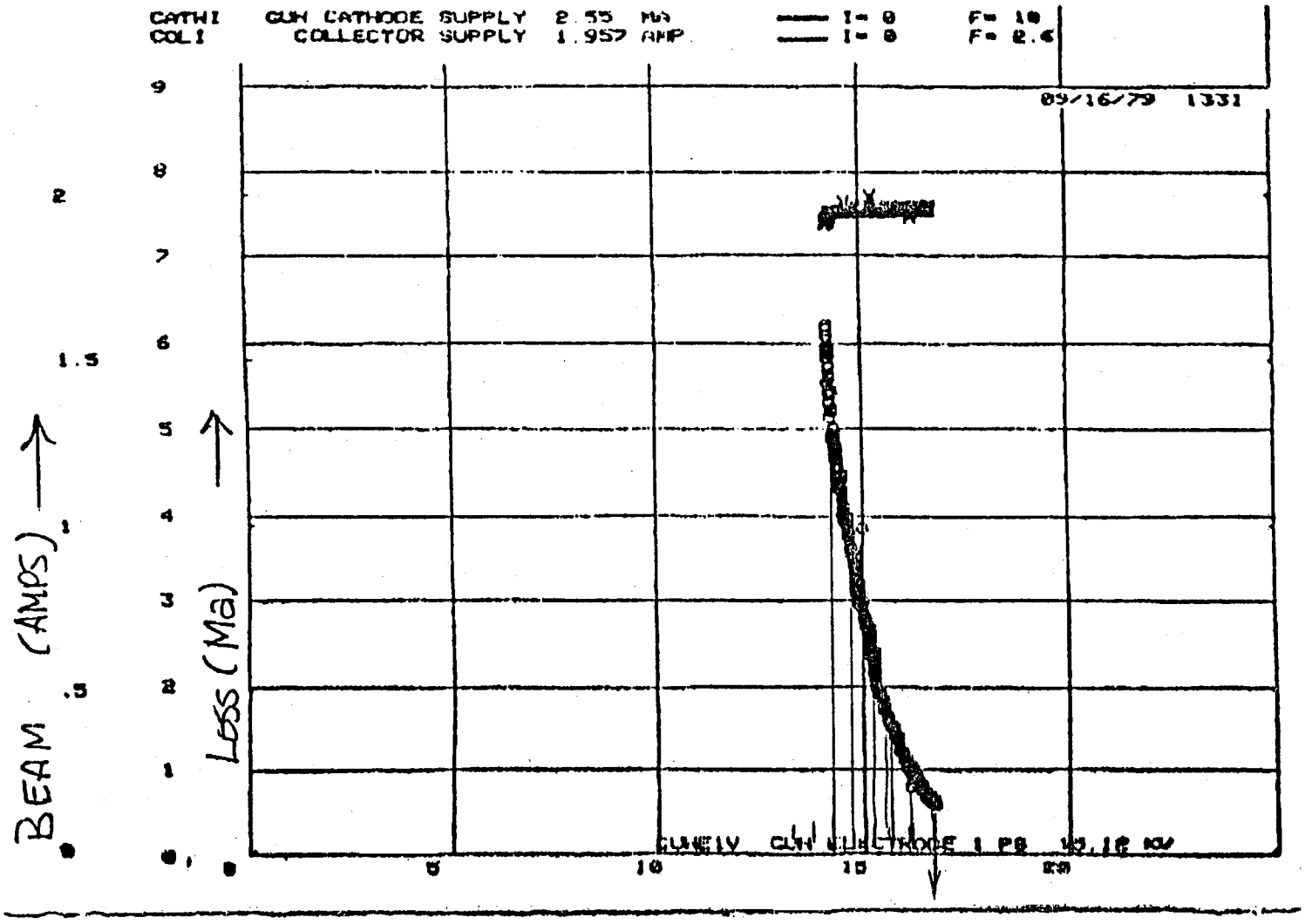
CATHI GUN CATHODE SUPPLY 2.55 MA
COLI COLLECTOR SUPPLY 1.957 AMP
I= 0
I= 0
F= 10
F= 2.6
09/16/79 1331
BEAM (AMPS)
Loss (Ma)
COLLECTOR ANODE VOLTAGE (KV)

Figure 4

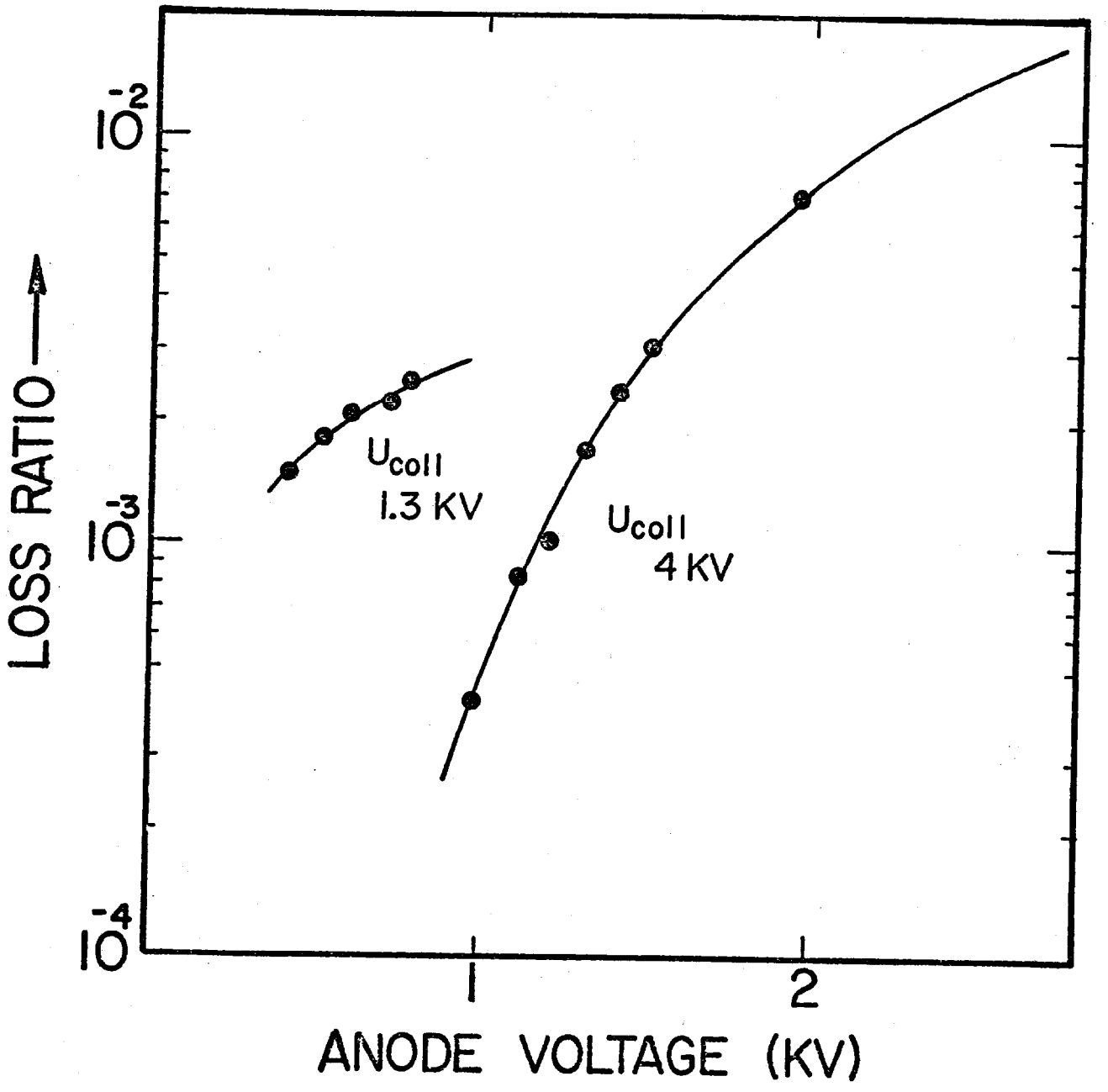
LOSS RATIO ⟶
10^{-2}
10^{-3}
10^{-4}
U_{coll}
1.3 KV
U_{coll}
4 KV
1
2
ANODE VOLTAGE (KV)

Figure 5

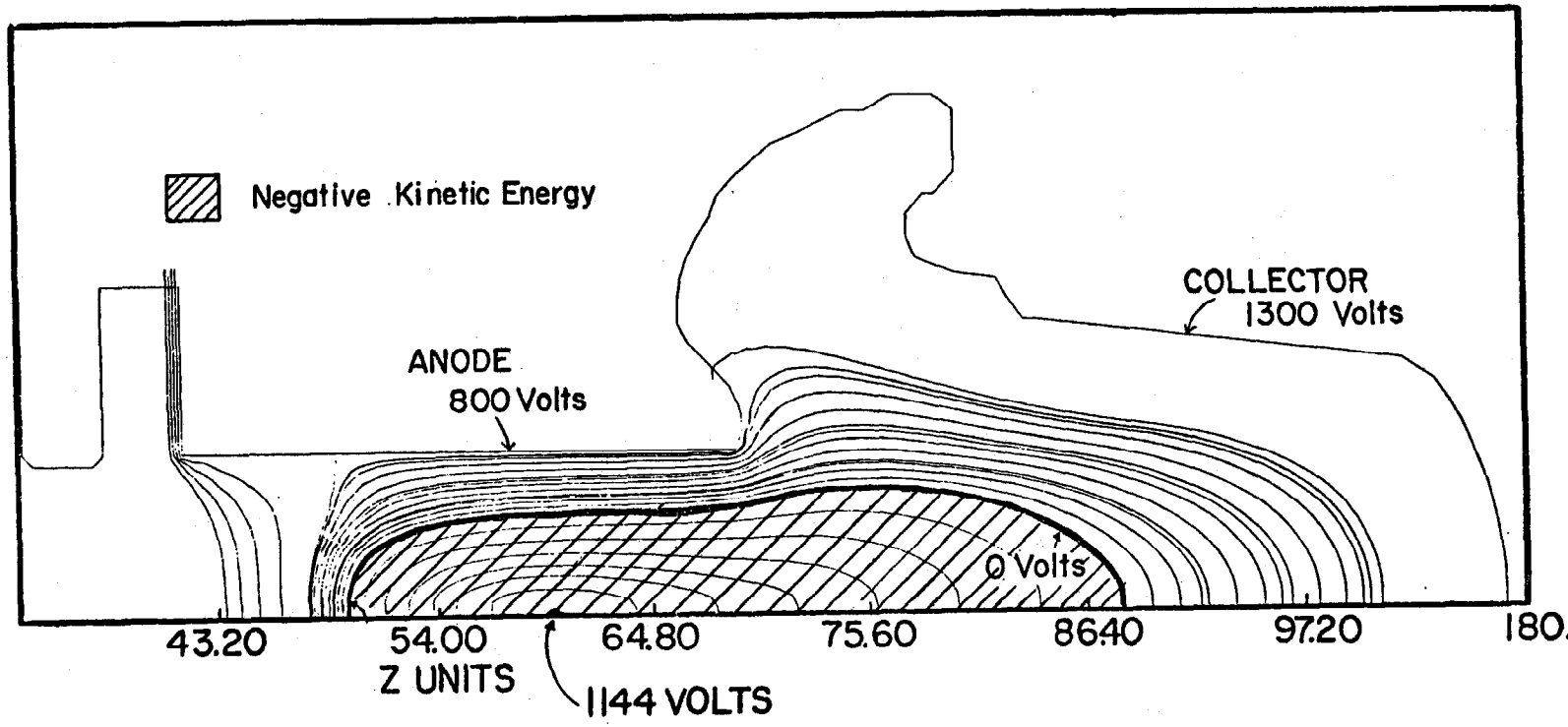
Negative Kinetic Energy
COLLECTOR
1300 Volts
ANODE
800 Volts
0 Volts
43.20
54.00
64.80
75.60
86.40
97.20
180.
Z UNITS
1144 VOLTS

Figure 6

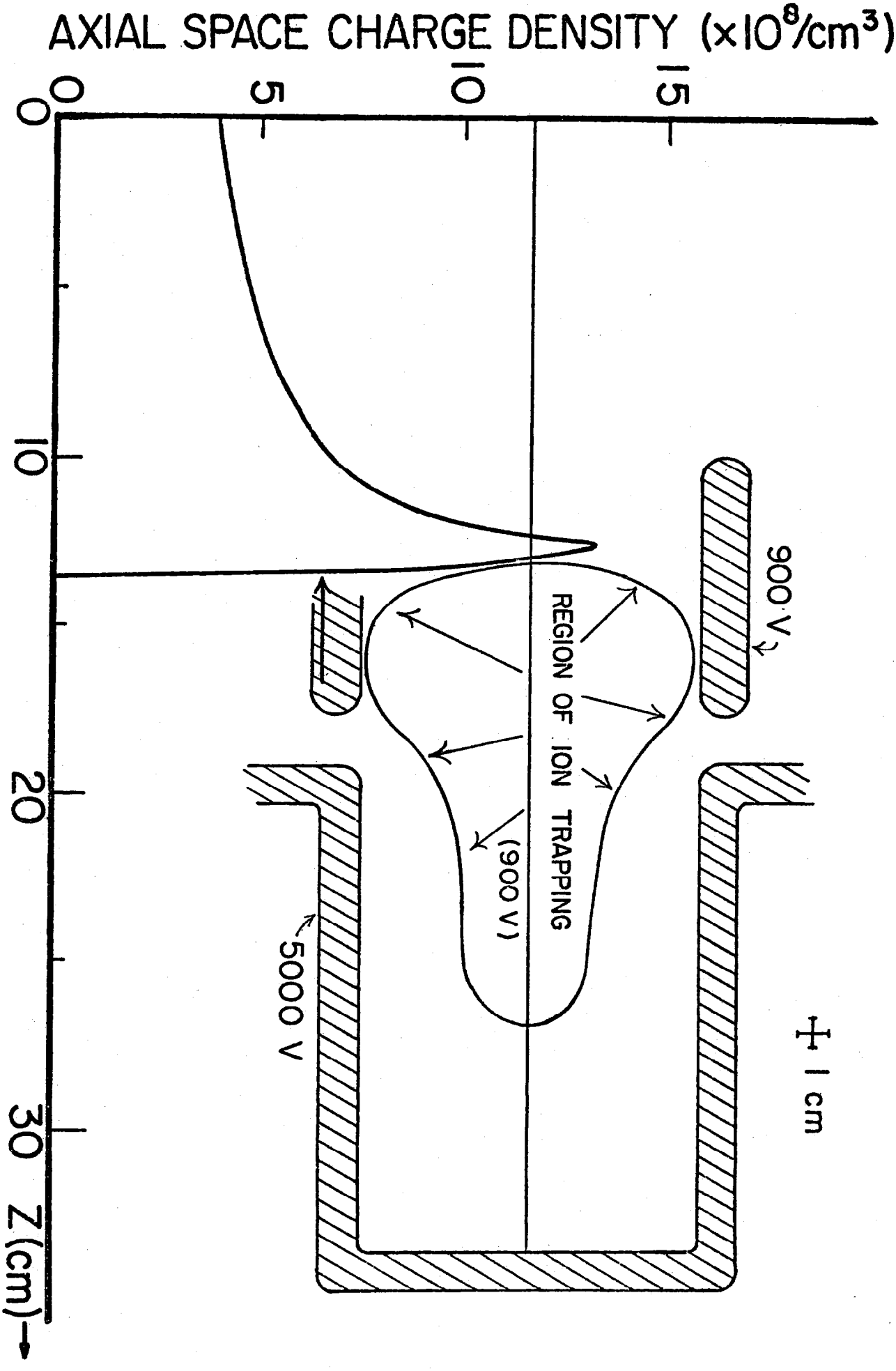
AXIAL SPACE CHARGE DENSITY (×10⁸/cm³)
0
5
10
15
0
10
20
30
Z(cm)
900 V
REGION OF ION TRAPPING
(900 V)
5000 V
1 cm

Figure 7

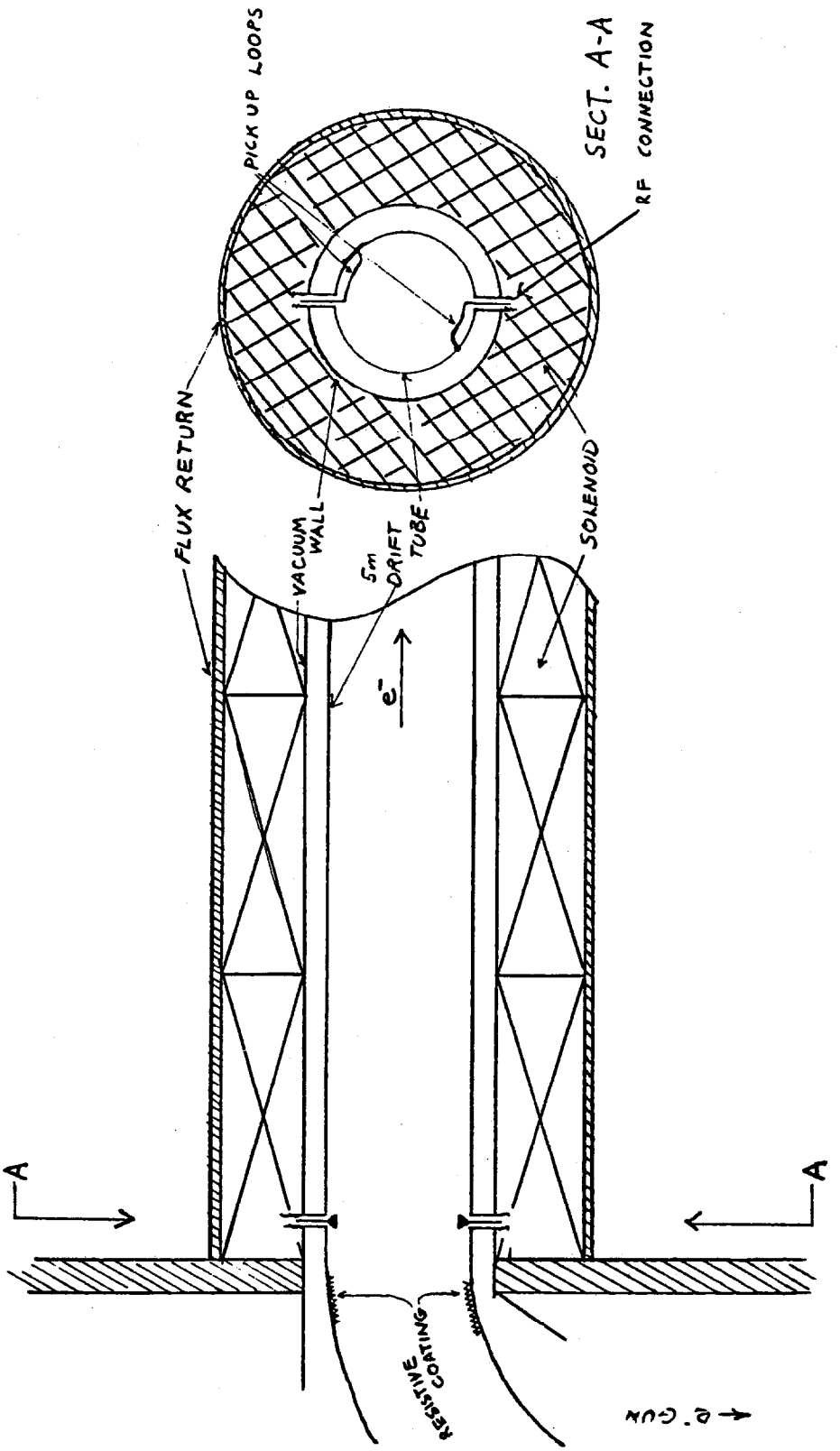
PICK UP LOOPS
SECT. A-A
RF CONNECTION
FLUX RETURN
VACUUM WALL
5m DRIFT TUBE
SOLENOID
e⁻
A
A
RESISTIVE COATING
e⁻ GUN

Figure 8

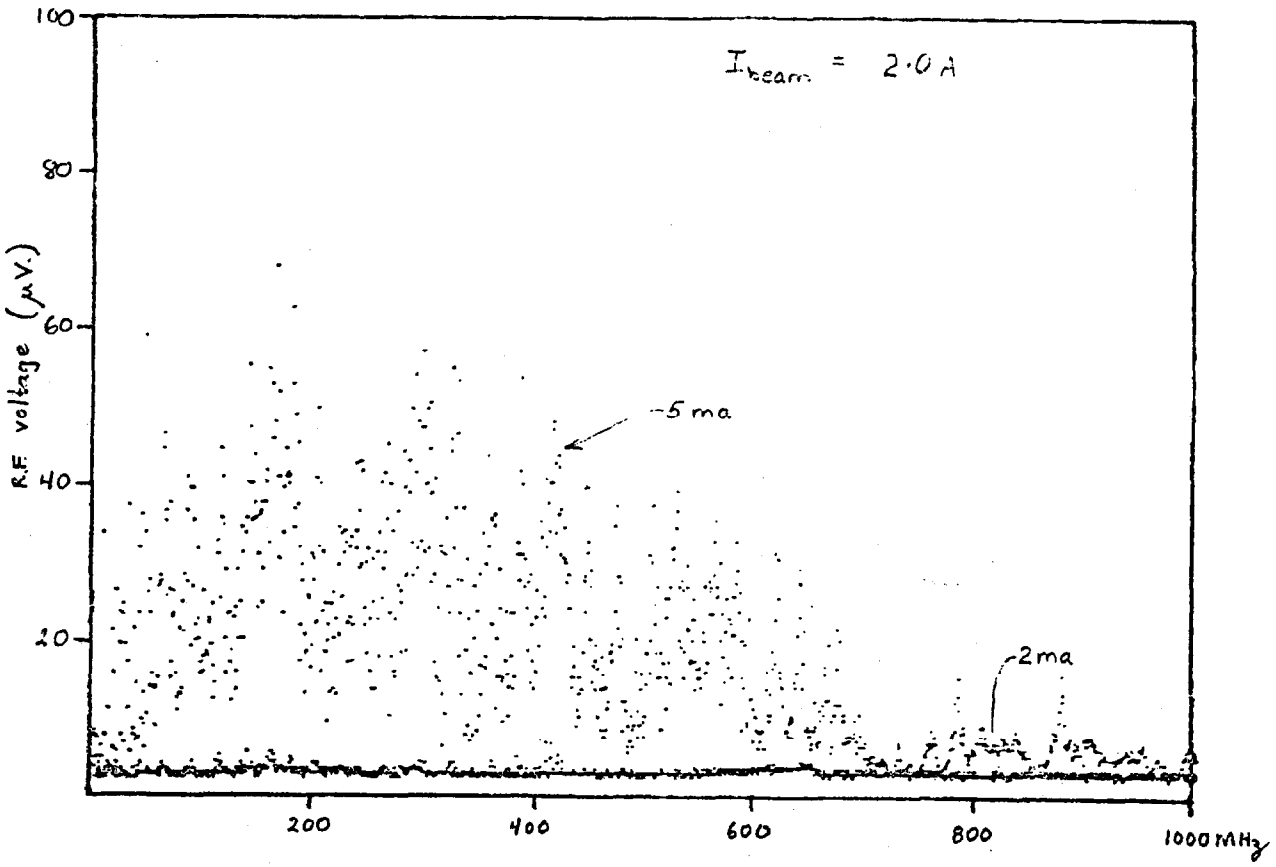

Figure 9

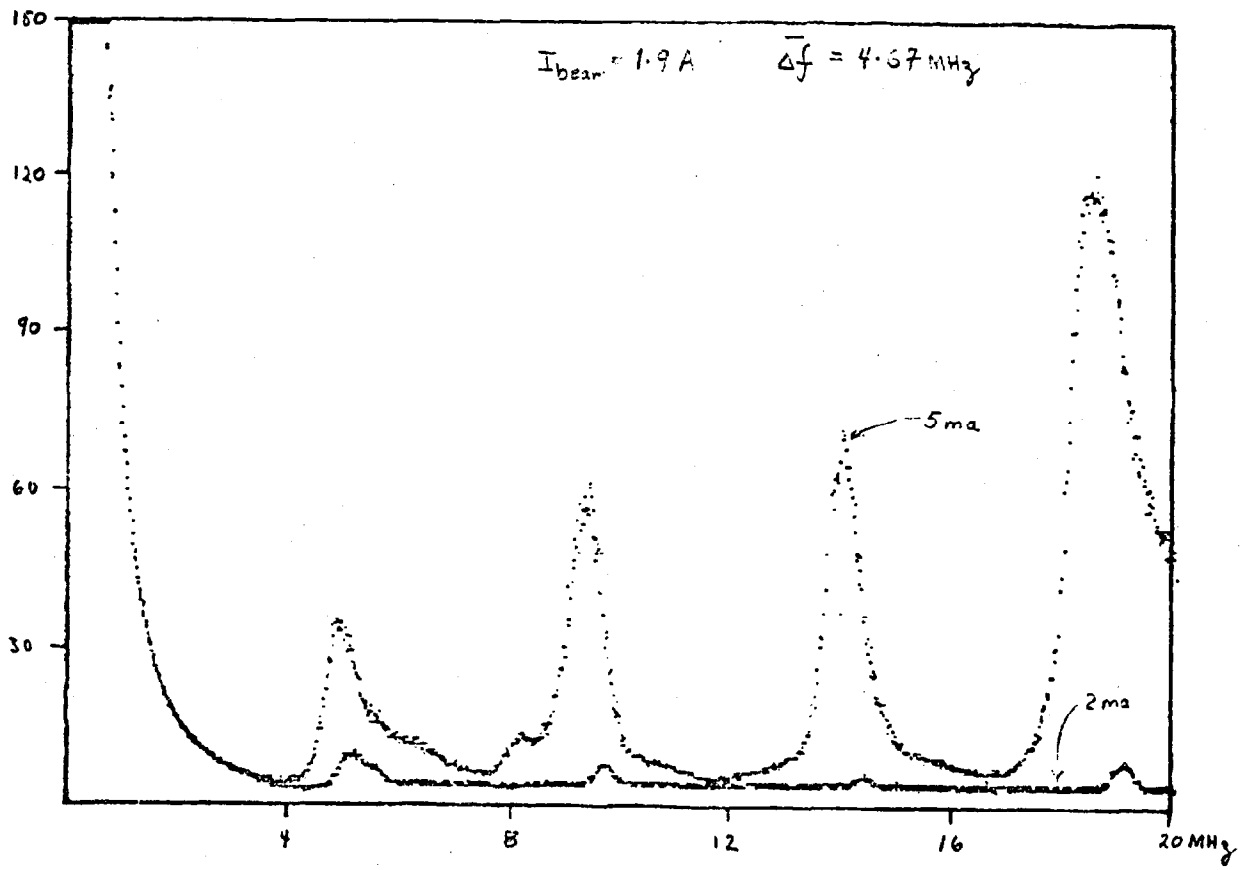

Figure 10

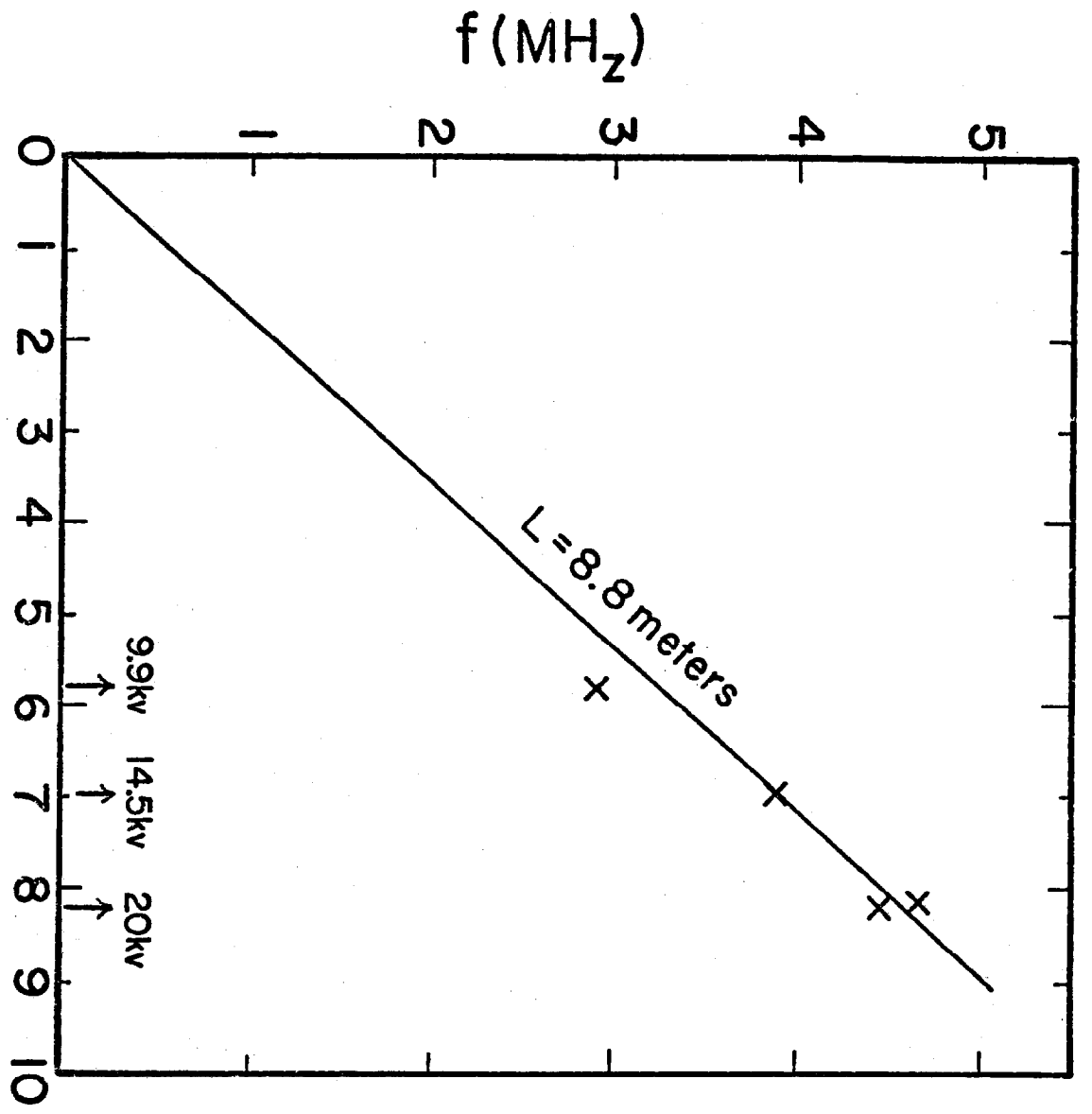
f(MHz)
1
2
3
4
5
0
1
2
3
4
5
6
7
8
9
10
$(v_o \times 10^{-9})$ cm/sec
L=8.8 meters
9.9kv
14.5kv
20kv

Figure 11

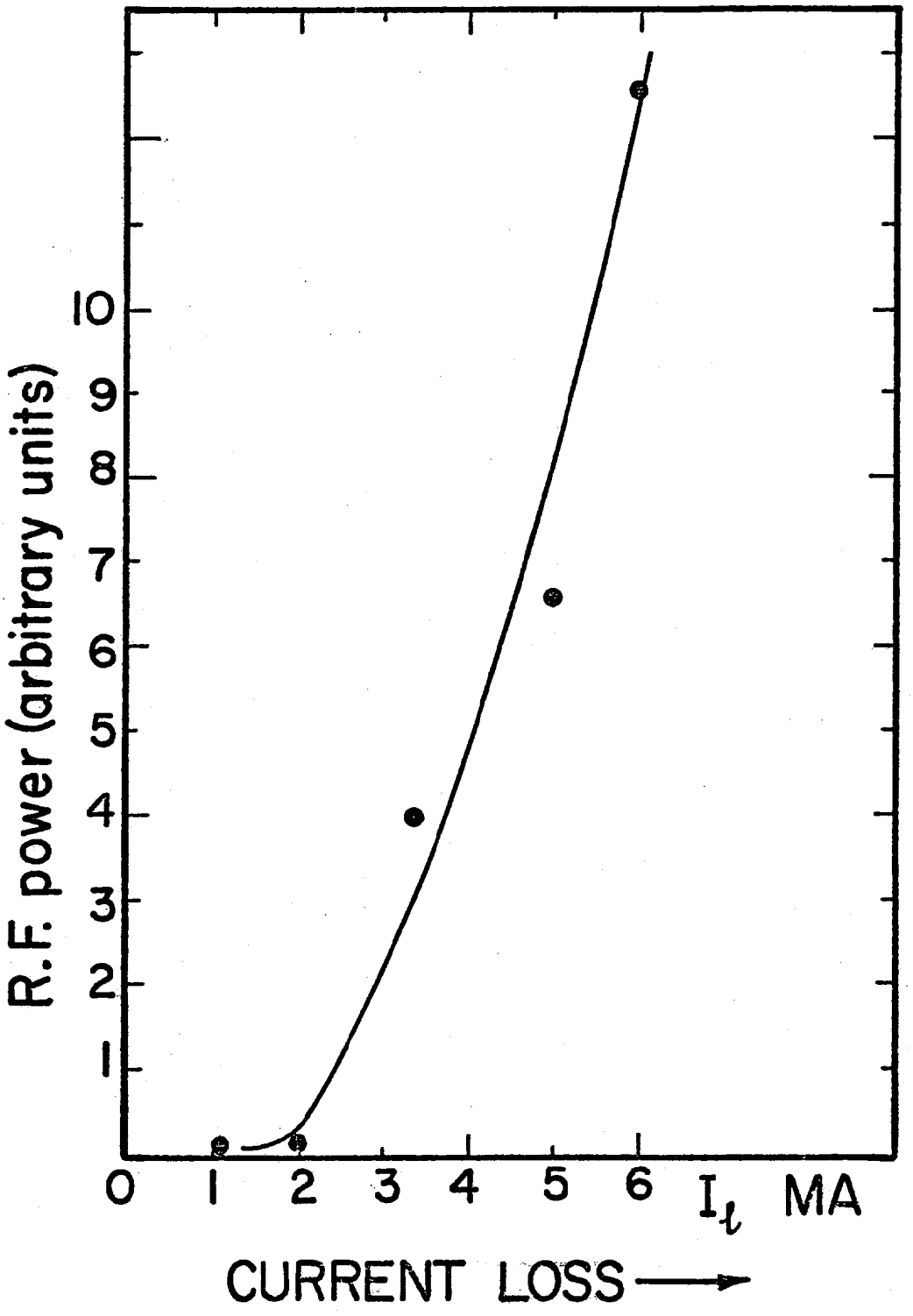
R.F. power (arbitrary units)
1
2
3
4
5
6
7
8
9
10
0
1
2
3
4
5
6
I_l MA
CURRENT LOSS ⟶

Figure 12

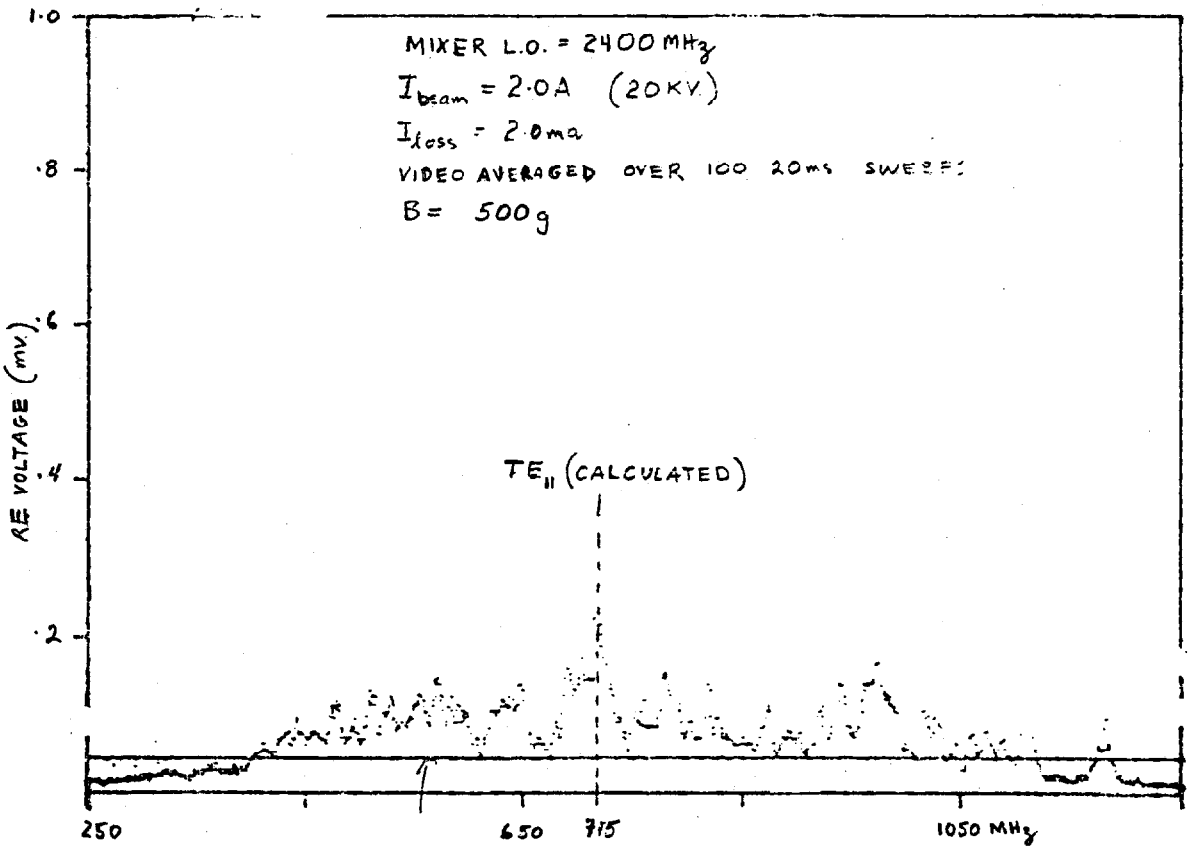
MIXER L.O. = 2400 MHz
I_{beam} = 2.0A (20KV)
I_{loss} = 2.0ma
VIDEO AVERAGED OVER 100 20ms SWEEPS
B = 500g
TE_{11} (CALCULATED)
AE VOLTAGE (mv)
1.0
.8
.6
.4
.2
250
650
715
1050 MHz

Figure 13